Monthly Notices of the ROYAL ASTRONOMICAL SOCIETY

MNRAS **479,** L108–L112 (2018)
Advance Access publication 2018 June 14

doi:10.1093/mnrasl/sly107

Radial distribution of stellar motions in *Gaia* DR2

Daisuke Kawata,[1★] Junichi Baba,[2] Ioana Ciucă,[1†] Mark Cropper,[1] Robert J. J. Grand,[3,4] Jason A. S. Hunt[5] and George Seabroke[1]

[1]*Mullard Space Science Laboratory, University College London, Holmbury St. Mary, Dorking, Surrey RH5 6NT, UK*
[2]*National Astronomical Observatory of Japan, Mitaka, Tokyo 181-8588, Japan*
[3]*Department of Astronomy and Astrophysics, University of Toronto, 50 St. George Street, Toronto, ON M5S 3H4, Canada*
[4]*Department of Astronomy, The University of Tokyo, 7-3-1 Hongo, Bunkyo-ku, Tokyo 113-0033, Japan*
[5]*Dunlap Institute for Astronomy and Astrophysics, University of Toronto, ON M5S 3H4, Canada*

Accepted 2018 June 11. Received 2018 June 09; in original form 2018 April 26

ABSTRACT

By taking advantage of the superb measurements of position and velocity for an unprecedented large number of stars provided in *Gaia* DR2, we have generated the first maps of the rotation velocity, $V_{\rm rot}$, and vertical velocity, $V_{\rm z}$, distributions as a function of the Galactocentric radius, $R_{\rm gal}$, across a radial range of $5 < R_{\rm gal} < 12$ kpc. In the $R - V_{\rm rot}$ map, we have identified many diagonal ridge features, which are compared with the location of the spiral arms and the expected outer Lindblad resonance of the Galactic bar. We have detected also radial wave-like oscillations of the peak of the vertical velocity distribution.

Key words: Galaxy: disc – Galaxy: evolution – Galaxy: kinematics and dynamics.

1 INTRODUCTION

Stellar velocity structure as a function of the Galactocentric radius, $R_{\rm gal}$, and the azimuthal position of the disc provides fruitful information about the impact of non-axisymmetric structures, such as the bar and spiral arms (e.g. Dehnen 2000; Kawata et al. 2014; Monari et al. 2016) and satellite galaxies (e.g. Gómez et al. 2012; D'Onghia et al. 2016) on the Galactic disc. Recent ground-based spectroscopic surveys of Galactic stars with multi-object spectrographs have demonstrated the complex structure of stellar velocity fields including the velocity fluctuation of the Galactic disc (e.g. Widrow et al. 2012; Bovy et al. 2015; Tian et al. 2017), asymmetric motions (e.g. Williams et al. 2013; Carrillo et al. 2018; Wang et al. 2018) and resonance features (e.g. Liu et al. 2012; Gómez et al. 2013; Tian et al. 2017). However, these studies are mainly based on the line-of-sight radial velocity only. Furthermore, the distance measurements rely on the photometric distance that is subject to dust extinction corrections.

The European Space Agency's *Gaia* mission (Gaia Collaboration 2016) has made their second data release (*Gaia* DR2; Gaia Collaboration 2018a) that provides the unprecedentedly accurate measurements of parallax and proper motion (Lindegren et al. 2018) and line-of-sight velocity of a large number of bright stars (Cropper et al. 2018; Katz et al. 2018; Sartoretti et al. 2018). This revolutionary data set provides 6D phase space information: the positions and velocities of stars, which allows us to measure the Galactic rotation, radial and vertical velocity structure in different regions of the Galactic disc, as demonstrated in Gaia Collaboration (2018b). The line-of-sight velocities are available only for the bright ($G < \sim$13 mag) stars in the *Gaia* DR2. However, for fainter stars accurate parallax and proper motions are still available. As demonstrated in Hunt et al. (2017) with the *Gaia* DR1, we can use the proper motion of the Galactic longitudinal direction, $V_{\rm l}$, as a proxy to the Galactic rotation velocity, $V_{\rm rot}$, in the direction of $l = 0$ and 180 deg and $b = 0$. Hunt et al. (2017) identified a fast rotating moving group that spreads over 0.6 kpc in radius, and demonstrated that the decreasing rotation velocity of the *Hercules* stream found in Monari et al. (2017) can be seen in $R_{\rm gal}$ versus $V_{\rm l}$ without the line-of-sight velocity information. Schönrich & Dehnen (2017) further analysed both $V_{\rm l}$ and velocity in the direction of the Galactic latitude, $V_{\rm b}$, as a proxy of vertical motion, $V_{\rm z}$, using the *Gaia* DR1 in the direction of $l = 0$ and $l = 180$ deg. They found that $\langle V_{\rm z}\rangle$ as a function of the guiding centre exhibits wave-like oscillations superposed on top of an overall increase with radius, which they interpret as a combination of vertical waves propagating radially and the warp of the disc.

In this *Letter*, we take advantage of the superb astrometric accuracy of *Gaia* DR2 to produce the first maps of $V_{\rm rot}(\sim V_{\rm l})$ and $V_{\rm z}(\sim V_{\rm b})$ distributions as a function of Galactocentric radius, covering the radial range $5 \lesssim R_{\rm gal} \lesssim 12$ kpc, in the direction of $l = 0$ and $l = 180$ and $b = 0$. We identify diagonal ridge features in $R - V_{\rm rot}$ map and wave-like features in the $R - V_{\rm z}$ map, and compare them with the location of the spiral arm and the resonance radii of the expected bar pattern speed.

★ E-mail: d.kawata@ucl.ac.uk
† LSSTC Data Science Fellow

Section 2 describes our data and sample selection. Section 3 shows our results. A summary and discussion of this study are presented in Section 4.

2 DATA AND ANALYSIS

We have extracted two different samples of stars from the *Gaia* DR2 catalogue in a volume within the width in the disc plane of 0.2 kpc and height from the plane within 0.2 kpc along the line of the Galactic centre and the Galactic anticentre. We assumed the Sun's Galactocentric radius of $R_0 = 8.2$ kpc and vertical offset from the Galactic mid-plane of $z_0 = 25$ pc. We also assumed the solar motion in the rotation direction of $V_\odot = 248\ \mathrm{km\,s^{-1}}$ which is faster than the rotation speed of the Local Standard of the Rest (LSR), V_{LSR} by $V_\odot = 11\ \mathrm{km\,s^{-1}}$. We also assumed the solar motion in the vertical direction of $W_\odot = 7.0\ \mathrm{km\,s^{-1}}$. These values are taken from Bland-Hawthorn & Gerhard (2016). Note that these values are set for convenience of presentation, and our results do not depend on these assumed values.

The first sample comprises stars whose line-of-sight velocity measured with the *Gaia*'s RVS instrument (Cropper et al. 2018) are available in the *Gaia* DR2. We also selected stars whose radial velocity uncertainties are smaller than $5\ \mathrm{km\,s^{-1}}$ and whose parallax accuracy is better than 15 per cent, i.e. $\varpi/\sigma_\varpi > 1/0.15$, where ϖ is parallax and σ_ϖ is its uncertainty. As mentioned above, we only selected stars within 0.2 kpc from the plane and 0.2 kpc perpendicular to the line of the Galactic centre and the Galactic anticentre. For this sample, the full 6D position and velocity information is available, and V_{rot} and V_{z} are derived with the assumed Galactic parameters shown above. We used GALPY (Bovy 2015) for all coordinate transformation. There are 861 680 stars in this sample. We call this sample the 'RVS' sample.

The second sample includes all stars brighter than $G = 15.2$ mag, but again with $\varpi/\sigma_\varpi > 1/0.15$. This sample has no line-of-sight velocity information in the *Gaia* DR2, except the bright stars with limited effective temperature values. Hence, we limit the sample to within $|b| < 10$ deg and $|l| < 10$ deg or $|l| - 180 < 10$ deg. Again, we only selected stars within 0.2 kpc from the plane and 0.2 kpc from the line of the Galactic centre and the Galactic anticentre. In this limited region, there are 1049 340 stars. We call this sample the 'All' sample. In this *Letter*, we assume that in this limited angular region $V_{\mathrm{l}} = V_{\mathrm{rot}}$ and $V_{\mathrm{b}} = V_{\mathrm{z}}$.

Using the mock data constructed with GALAXIA (Sharma et al. 2011), we estimated that the average difference between V_{l} and V_{rot} is about $0.3\ \mathrm{km\,s^{-1}}$. However, the average differences depend on l and it increases to about $2.7\ \mathrm{km\,s^{-1}}$ at $|l| = 10$ deg or $|l - 180| = 10$ deg. Because we discuss the V_{rot} distribution as a function of R_{gal} by summing the contribution from all the stars with different l, this systematic dependence on l should not affect our results. The average difference between V_{b} and V_{z} is smaller than $0.4\ \mathrm{km\,s^{-1}}$, and we do not find any correlation with l. This is consistent with what is shown in Schönrich & Dehnen (2017).

3 RESULTS

3.1 R_{gal} versus V_{rot}

Fig. 1 shows the distribution of $V_{\mathrm{rot}} - V_{\mathrm{LSR}}$ as a function of R_{gal} for our two samples of stars. Because each sample has a different number of stars distributed in different radial bins, we normalized the distribution at each radial bin to highlight the features in the velocity distribution. Because the brightness limits are different for each sample, the radial range covered by each sample is different; stars in our 'All' sample reach up to ∼4 kpc from the Sun, whereas stars in our 'RVS' sample are confined to a slightly smaller volume. It is striking to see many diagonal ridge-like features, highlighted by white diagonal lines. To our knowledge, this is the first time that these clear features are seen in observational data, and this is a new window opened up by *Gaia*. Features are more clear in our 'All' sample (except F1, F2, and F3 that are more clear and selected in the 'RVS' sample around the solar radius), and are therefore selected by eye in the 'All' sample panel. The 'All' sample includes fainter stars and there are more stars closer to the disc mid-plane. Therefore, more features are visible in this sample. F1 and F2 correspond to the split Hercules streams (see also Gaia Collaboration 2018b; Antoja et al. 2018; Trick, Coronado & Rix 2018), which are highlighted in the upper panel. F3 is due to the so-called Hyades and Pleiades moving groups, and F4 corresponds to the Sirius moving group (see also Ramos, Antoja & Figueras 2018). F2, F3, F4, and F5 are highlighted between $V_{\mathrm{rot}} - V_{\mathrm{LSR}} = 20$ and $-40\ \mathrm{km\,s^{-1}}$, because most of the features cover this velocity range, although some features extend to higher velocity. F1 extends to lower velocities, which is clearly visible in the 'RVS' sample. F6 and F7 are highlighted only in the range visible in the 'All' sample.

The vertical dashed lines in Fig. 1 show the position of the spiral arms at $y = 0$. The positions are calculated from what is measured in Reid et al. (2014) and scaled to our assumed $R_0 = 8.2$ kpc. Each line corresponds to the Scutum, Sagittarius, Local, and Perseus spiral arms from left to right. We can see the two split inclined features with systematically higher and lower rotation velocity than the LSR rotation speed at the location of Perseus arms (F6 and F7). Although it is tentative, especially in the 'All' sample the rotation velocity in the inside of the Scutum arm is clearly slower than that in the outside of the arm. These bimodal features either side of the LSR rotation speed are expected around the spiral arm at the corotation resonance (e.g. Kawata et al. 2014). If these are from corotation of the spiral arms, this indicates that the Scutum and Perseus arms have different pattern speeds, which can be naturally explained if these spiral arms are corotating at every radius, as seen in recent *N*-body simulations (Wada, Baba & Saitoh 2011; Grand, Kawata & Cropper 2012a,b; Baba, Saitoh & Wada 2013). However, to test the spiral arm scenario, we need to look at V_{rot} distribution in a larger region of the disc (Hunt et al. 2015; Hunt et al. 2018; Quillen et al. 2018).

There is similar bimodal feature around the Local arm (F3 and F4). The slope of this feature ($\mathrm{d}V_{\mathrm{rot}}/\mathrm{d}R \sim -28\ \mathrm{km\,s^{-1}\ kpc^{-1}}$) looks steeper than the one in the Perseus arms ($\mathrm{d}V_{\mathrm{rot}}/\mathrm{d}R \sim -9\ \mathrm{km\,s^{-1}\ kpc^{-1}}$). The Local arm is often considered to be a weak spiral arm or spur, and it is not expected to influence the stellar motion as strongly as the main spiral arms, like the Scutum and Perseus arms where clear stellar density enhancements are observed. Hence, we expect that the origins of F3 and F4 are not related to the spiral arms (but see Quillen et al. 2018, for an alternative view explaining these features with the Local arm and the Local spur).

Compared to the Scutum and Perseus arms, there is no such feature at the radius of the Sagittarius arm, except the extension of F1 and F2. Therefore, we speculate that these arms are not stellar arms, but only gaseous star-forming arms, as indicated in Benjamin et al. (2005), who found no significant density enhancement at the position of the Sagittarius arm in the *Spitzer* GLIMPSE survey. In this case, the spiral arms may not have enough gravitational potential to influence the stellar motions. If this is true, our results support $m = 2$ spiral arms in the Milky Way, which is in fact more common in a barred galaxy (e.g. Hart et al. 2017).

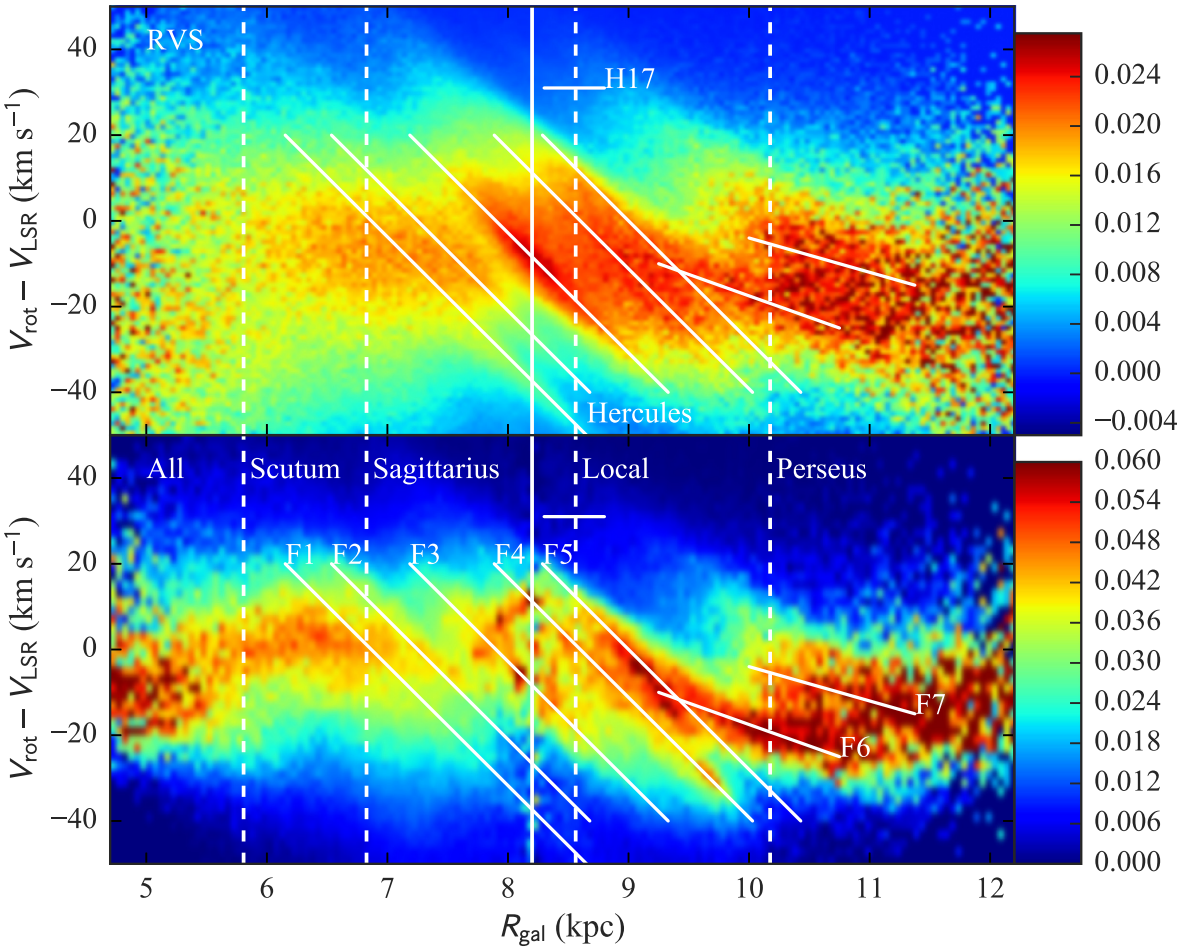

Figure 1. Normalized distribution of the rotation velocity for our RVS stars (upper) and our All stars (lower) as a function of the Galactocentric radius. The vertical dashed lines show the position of the Scutum, Sagittarius, Local, and Perseus spiral arms from left to right, which are calculated from Reid et al. (2014). The vertical solid line is the assumed solar radius. The white lines highlight the identified ridge features.

We also note that we can see also a group of stars (indicated as 'H17' in the upper panel of Fig. 1) with high rotation velocities just outside of R_0, which were found in Hunt et al. (2017). However, they are not a horizontal feature as suggested in Hunt et al. (2017), but rather form a diagonal feature parallel to F5 with a higher rotation speed in the 'RVS' sample. This feature is tentative, therefore we do not select it as a clear diagonal feature. We note that this feature seems to be connected to the 'Arch 1' feature in the solar neighbourhood velocity distribution, highlighted in the wavelet analysis in Ramos et al. (2018), although they do not find any extension of the feature to regions outside of the solar radius. Nevertheless, it will be interesting to study this feature further using future *Gaia* data releases.

Fig. 1 also traces the whole resonance feature of the Hercules stream. With the *Gaia* DR1 and LAMOST data, Monari et al. (2017) found the rotation speed of the Hercules stream ($V_{rot} - V_{LSR} \sim -30$ to -40 km s^{-1} at $R = R_0$) decreases with radius for $R_{gal} > R_0$, and therefore the gap between the Hercules stream and the Hyades and Pleiades moving groups (F3 in Fig. 1) decreases with radius. It is expected that the gap should extend to the inner disc (Antoja et al. 2014) and that the rotation speed of the Hercules stream increases with decreasing R_{gal}. For the first time, the *Gaia* DR2 has revealed the inner extension of the gap due to the Hercules stream as a clear gap between F2 and F3 in Fig. 1. This gap crosses the V_{LSR} at R_{gal} ~ 7.6 kpc. This could be the outer Lindblad resonance (OLR) of the fast rotating bar, as widely believed (Dehnen 2000; Monari et al. 2017). However, we note that there are many mechanisms that can explain the Hercules stream feature (e.g. Hattori et al. 2018; Hunt & Bovy 2018), and examining the velocity distribution in a larger region of the disc is necessary to determine the pattern speed of the bar and the location of its resonances.

3.2 R_{gal} versus V_z

Fig. 2 shows the distribution of V_z as a function of R_{gal} for our three samples of stars. We again normalized the distribution at each radial bin to highlight the features in the distribution. We do not find any features like the ridge features in V_{rot}. Instead, the mean velocity shows wave-like oscillations and increases with R_{gal}. To trace the centroid of the velocity distribution, we selected stars within 0.2 kpc from radial grid points at every 0.2 kpc in R_{gal}, i.e. each grid point has 0.1 kpc of overlap region with their neighbour points, and hence every second grid point is independent. At each radial bin, we fit the velocity distribution with two Gaussians using extreme-deconvolution (Bovy, Hogg & Roweis 2011). We estimated the uncertainty of V_z (or V_b) by taking 1000 Monte-Carlo (MC) samples of the parallax and proper motion with their uncertainties and correlations for each star, converting them to V_z (or V_b) and

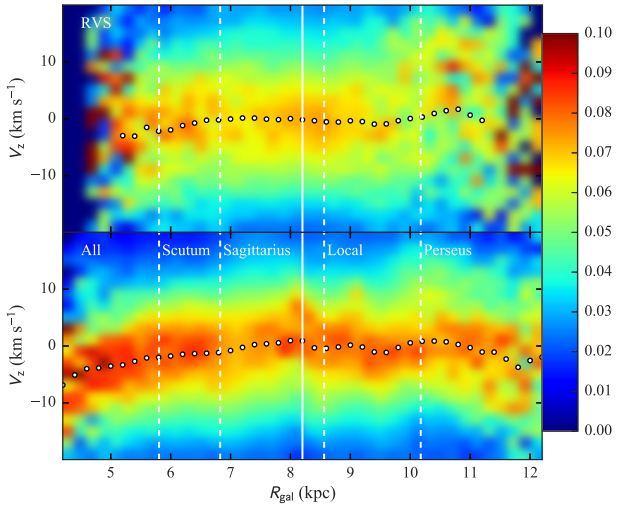

Figure 2. Distribution of the vertical velocity for the 'RVS' stars (upper) and stars in the 'All' sample (lower) as a function of Galactocentric radius. The symbols indicate the peak of the density at each radius. The circles show the stronger peak detected with two Gaussian models. The vertical dashed lines show the position of the Scutum, Sagittarius, Local, and Perseus spiral arms from left to right, as suggested in Reid et al. (2014). The vertical solid line indicates the solar radius.

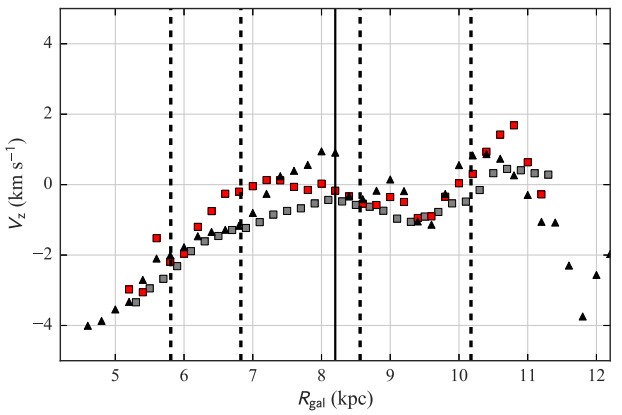

Figure 3. The mean vertical velocity of the most significantly identified feature in Fig. 2. Red squares and black triangles are the results for the 'RVS' sample and the 'All' sample, respectively. For a reference, grey squares show the median V_z for the 'RVS' sample.

taking the standard deviation. Using different numbers of Gaussian models, we find that two Gaussians is the optimal and most robust choice to trace the peak of the velocity distribution. Fig. 3 shows that the position of the mean of the main Gaussian model, which show a clear oscillatory pattern (see also fig. 14 Gaia Collaboration 2018b, who showed similar results for the 'RVS' sample in more detail). Interestingly, the results for the 'All' sample are similar to what is seen in 'basic method' of fig. 9 in Schönrich & Dehnen (2017). The peaks of the oscillatory pattern in Fig. 3 are around $R_{gal} = 8$ and 10.5 kpc, and the dip is around $R_{gal} = 9$ kpc with a small spike, which are similar in locations of the peak, dip, and spike found in Schönrich & Dehnen (2017), although they used the guiding centre to detect these trends from the local sample of the *Gaia* DR1. This oscillatory pattern is superposed on top of a clear increase in V_z with R_{gal}, which is suggestive of a warp in the outer disc as discussed in Schönrich & Dehnen (2017), and consistent with the predicted vertical waves induced by the Sagittarius dwarf galaxy in Gómez et al. (2013).

Interestingly, our 'RVS' sample shows a similar oscillatory pattern, but it has a slightly longer wavelength. As mentioned above, the 'All' sample contains more stars closer to the disc mid-plane compared to the 'RVS' sample. We wildly speculate that this may indicate that stars in the denser plane have shorter wavelength than the stars above the plane, or that there may be multiple modes of the waves propagating differently for different stellar populations.

Note that the grey squares in Fig. 3 show the median V_z for the 'RVS' sample as a comparison to the mean of the main Gaussian model shown with red squares. The median V_z also shows the oscillatory pattern. However, the amplitude is smaller and the spike at $R_{gal} = 9$ kpc is not seen. Hence, we think that deconvolution of the velocity distribution is important to get rid of the kinematically hot component, like halo and thick disc stars, and highlight the main velocity features in the thin disc.

4 SUMMARY

By taking advantage of the unprecedented precise astrometric measurements of a large number of stars provided by the *Gaia* DR2, we have generated the first maps of the $R - V_{rot}$ and $R - V_z$ covering a radial range of 5 to 12 kpc in Galactocentric radius along the Galactic centre and Galactic anticentre line-of-sight. We discovered many diagonal ridge features in the $R - V_{rot}$ map. Some of these are likely related to the perturbations from the bar's OLR and spiral arm. Alternatively, as suggested in Antoja et al. (2018), some of these features could be due to phase wrapping (Minchev et al. 2009; Gómez et al. 2012). We found the transition of V_{rot} between the inside and the outside of the Scutum and Perseus arms. We speculate that these features are due to corotation resonances of the spiral arms, which may be explained with the transient spiral arm scenario. There are several ridge features around the solar neighbourhood/Local arm, but the features are steeper compared to the ridges around the Perseus arm. We speculate that ridges of different slopes have different origins, and more theoretical works are required to explain these features.

In the $R - V_z$ distribution, we found the peak of the V_z distribution shows wave-like features almost identical to those seen in the local sample of *Gaia* DR1 in Schönrich & Dehnen (2017). The origin of the wave modes must be tightly related to the formation and evolution of the Galaxy (e.g. Widrow et al. 2012; Gómez et al. 2013; de la Vega et al. 2015; Xu et al. 2015; Gómez et al. 2017, among others), and comparisons between these observations and models are urgently required.

ACKNOWLEDGEMENTS

We thank an anonymous referee for his constructive comments and helpful suggestions which have improved the manuscript. DK, IC, MC, and GS acknowledge the support of the UK's Science & Technology Facilities Council (STFC Grant ST/N000811/1). JB is supported by the Japan Society for the Promotion of Science (JSPS) Grant-in-Aid for Scientific Research (C) Grant number 18K03711. IC is also grateful for the STFC Doctoral Training Partnerships Grant (ST/N504488/1). RJJG acknowledges support by the DFG Research Centre SFB-881 'The Milky Way System', through project A1. JH is supported by a Dunlap Fellowship at theDunlap Institute for Astronomy & Astrophysics, funded through an endowment established by the Dunlap family and the University of Toronto. This work was inspired from

our numerical simulation studies used at the UCL facility Grace and the DiRAC Data Analytic system at the University of Cambridge, operated by the University of Cambridge High Performance Computing Service on behalf of the STFC DiRAC HPC Facility (www.dirac.ac.uk). This equipment was funded by BIS National E-infrastructure capital grant (ST/K001590/1), STFC capital grants ST/H008861/1, and ST/H00887X/1, and STFC DiRAC Operations grant ST/K00333X/1. DiRAC is part of the National E-Infrastructure. This work has made use of data from the European Space Agency (ESA) mission *Gaia* (https://www.cosmos.esa.int/gaia), processed by the *Gaia* Data Processing and Analysis Consortium (DPAC, https://www.cosmos.esa.int/web/gaia/dpac/consortium). Funding for the DPAC has been provided by national institutions, in particular the institutions participating in the *Gaia* Multilateral Agreement.

REFERENCES

Antoja T. et al., 2014, A&A, 563, A60
Antoja T. et al., 2018, preprint (arXiv:1804.10196)
Baba J., Saitoh T. R., Wada K., 2013, ApJ, 763, 46
Benjamin R. A. et al., 2005, ApJ, 630, L149
Bland-Hawthorn J., Gerhard O., 2016, ARA&A, 54, 529
Bovy J., 2015, ApJS, 216, 29
Bovy J., Hogg D. W., Roweis S. T., 2011, Ann. Appl. Stat., 5, 1657
Bovy J., Bird J. C., García Pérez A. E., Majewski S. R., Nidever D. L., Zasowski G., 2015, ApJ, 800, 83
Carrillo I. et al., 2018, MNRAS, 475, 2679
Cropper M. et al., 2018, preprint (arXiv:1804.09369)
D'Onghia E., Madau P., Vera-Ciro C., Quillen A., Hernquist L., 2016, ApJ, 823, 4
de la Vega A., Quillen A. C., Carlin J. L., Chakrabarti S., D'Onghia E., 2015, MNRAS, 454, 933
Dehnen W., 2000, AJ, 119, 800
Gaia Collaboration, 2018a, preprint (arXiv:1804.09365)
Gaia Collaboration, 2016, A&A, 595, A1
Gaia Collaboration, 2018b, preprint (arXiv:1804.09380)
Gómez F. A., Minchev I., Villalobos Á., O'Shea B. W., Williams M. E. K., 2012, MNRAS, 419, 2163
Gómez F. A., Minchev I., O'Shea B. W., Beers T. C., Bullock J. S., Purcell C. W., 2013, MNRAS, 429, 159
Gómez F. A., White S. D. M., Grand R. J. J., Marinacci F., Springel V., Pakmor R., 2017, MNRAS, 465, 3446
Grand R. J. J., Kawata D., Cropper M., 2012a, MNRAS, 421, 1529
Grand R. J. J., Kawata D., Cropper M., 2012b, MNRAS, 426, 167
Hart R. E. et al., 2017, MNRAS, 472, 2263
Hattori K., Gouda N., Yano T., Sakai N., Tagawa H., Baba J., Kumamoto J., 2018, preprint (arXiv:1804.01920)
Hunt J. A. S., Bovy J., 2018, MNRAS, 477, 3945
Hunt J. A. S., Kawata D., Grand R. J. J., Minchev I., Pasetto S., Cropper M., 2015, MNRAS, 450, 2132
Hunt J. A. S., Kawata D., Monari G., Grand R. J. J., Famaey B., Siebert A., 2017, MNRAS, 467, L21
Hunt J. A. S., Hong J., Bovy J., Kawata D., Grand R. J. J., 2018, MNRAS, submitted
Katz D. et al., 2018, preprint (arXiv:1804.09372)
Kawata D., Hunt J. A. S., Grand R. J. J., Pasetto S., Cropper M., 2014, MNRAS, 443, 2757
Lindegren L. et al., 2018, preprint (arXiv:1804.09366)
Liu C., Xue X., Fang M., van de Ven G., Wu Y., Smith M. C., Carrell K., 2012, ApJ, 753, L24
Minchev I., Quillen A. C., Williams M., Freeman K. C., Nordhaus J., Siebert A., Bienaymé O., 2009, MNRAS, 396, L56
Monari G., Famaey B., Siebert A., Grand R. J. J., Kawata D., Boily C., 2016, MNRAS, 461, 3835
Monari G., Kawata D., Hunt J. A. S., Famaey B., 2017, MNRAS, 466, L113
Quillen A. C. et al., 2018, preprint (arXiv:1805.10236)
Ramos P., Antoja T., Figueras F., 2018, preprint (arXiv:1805.09790)
Reid M. J. et al., 2014, ApJ, 783, 130
Sartoretti P. et al., 2018, preprint (arXiv:1804.09371)
Schönrich R., , Dehnen W., 2018, MNRAS, 478, 3809,
Sharma S., Bland-Hawthorn J., Johnston K. V., Binney J., 2011, ApJ, 730, 3
Tian H.-J. et al., 2017, Res. Astron. Astrophys., 17, 114
Trick W. H., Coronado J., Rix H.-W., 2018, preprint (arXiv:1805.03653)
Wada K., Baba J., Saitoh T. R., 2011, ApJ, 735, 1
Wang H., López-Corredoira M., Carlin J. L., Deng L., 2018, MNRAS, 477, 2858,
Widrow L. M., Gardner S., Yanny B., Dodelson S., Chen H.-Y., 2012, ApJ, 750, L41
Williams M. E. K. et al., 2013, MNRAS, 436, 101
Xu Y., Newberg H. J., Carlin J. L., Liu C., Deng L., Li J., Schönrich R., Yanny B., 2015, ApJ, 801, 105

This paper has been typeset from a TEX/LATEX file prepared by the author.